Can Elastic Instability be Beneficial in Concentric Tube Robots?

Katherine E. Riojas†, *Student Member, IEEE*, Richard J. Hendrick†, *Member, IEEE* and Robert J. Webster III, *Senior Member, IEEE*

***Abstract*—Concentric tube manipulators exhibit elastic instability in which tubes snap from one configuration to another, rapidly releasing stored strain energy. While this has long been viewed as a negative phenomenon to be avoided at all costs, in this paper we explore for the first time whether the effect can be harnessed beneficially for certain applications. Specifically, we show that the energy released in an instability can be useful for challenging, high-force surgical tasks such as driving a needle through tissue. We use concentric tube models to define the energy released during elastic instability and experimentally evaluate a two-tube concentric manipulator that can drive suture needles through tissue by harnessing elastic instability beneficially.**

***Index Terms*—Medical Robots and Systems, Surgical Robotics: Laparoscopy**

I. Introduction

CONCENTRIC tube robots have been studied primarily as manipulators for surgical applications where fine control, dexterity, and accuracy are desirable. Because of this, elastic instability, where the manipulator suddenly releases strain energy and jumps from one configuration to another, has been viewed as an undesirable property of these manipulators. A number of prior studies have devised ways to avoid them through tube design [1], [2], [3], [4], [5], path planning [6], [7], and/or control [8], [9]. However, these instabilities have never previously been viewed as potentially beneficial, which is the perspective we take in this paper. Since an elastic instability rapidly releases a potentially large amount of energy, high power is available to be delivered to surgical tasks if it can be harnessed appropriately.

There has been rapid recent advancement in the study of elastic instability in concentric tube robots, and the mechanics-based model that describes them [10], [11] has recently been studied in depth to characterize elastic instability [12], [13]. Here, we use this theory to create a prototype manipulator that can drive a curved suturing needle through tissue by harnessing the energy released during an elastic instability.

This paper was recommended for publication by Editor K. Masamune upon evaluation of the Associate Editor and Reviewer's comments. This material is based upon work supported by the the National Institutes of Health under R01 EB017467 and the National Science Foundation Graduate Research Fellowship under DGE-1445197. Any opinions, findings, and conclusions or recommendations expressed in this material are those of the authors and do not necessarily reflect the views of the National Institutes of Health or the National Science Foundation.

K. E. Riojas, R. J. Hendrick, and R. J. Webster III are with the Vanderbilt Department of Mechanical Engineering, Vanderbilt University, Nashville, TN USA, {katherine.e.riojas, richard.j.hendrick, robert.webster}@vanderbilt.edu.
†K. E. Riojas and R. J. Hendrick contributed equally to this work.

Digital Object Identifier (DOI): see top of this page.

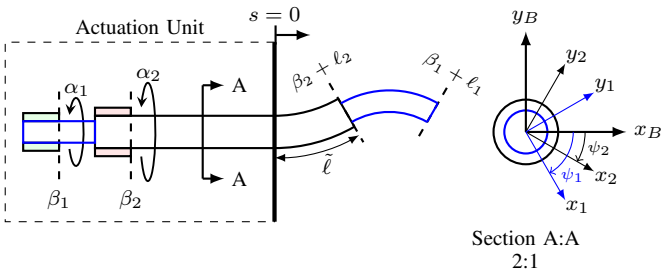

Fig. 1: Model parameters, kinematic variables, and coordinate frames for the concentric tube model.

To accomplish this task, we first provide the modeling background necessary to describe the kinematics, mechanics, and energy release that occur during elastic instability. We then use the model to create three concentric tube robots that can perform the rotational tip motion needed to drive sutures without significant Cartesian tip motion. We experimentally evaluate the performance of these three robots in benchtop experiments to explore average power release and repeatability of snap angle.

II. Modeling Elastic Instability

The purpose of this section is to provide the equations, based on the accepted mechanics and stability models (e.g. [10], [11], [12], [13]), that define the strain energy released during elastic instability. We restrict our analysis to two tube manipulators made from component tubes with straight lengths and constant precurvature tips, and many of the equations in this section have been simplified under these assumptions. The most general formulations can be found in the previous modeling work, cited above.

A. Frame Assignments and Kinematic Variables

We identify the index of the component tube with the subscript i, where $i = 1$ and $i = 2$ correspond to the inner and outer tube, respectively. We assume that each component tube has a total length ℓ_i and is straight except for a constant precurvature tip of precurvature κ_i. The model assumes that the cross-section of each tube remains annular during bending, and we define the bending and torsional stiffness of the component tubes as k_{ib} and k_{it}, respectively.

We assume that there are material-attached frames $\boldsymbol{g}_1(s)$ and $\boldsymbol{g}_2(s)$ attached to the inner and outer tube, respectively, at every arc length and that there is a Bishop frame attached to the backbone of the manipulator. The z-axes of each of these frames are aligned and tangent to the backbone, but

TABLE I: Kinematic Symbols

$\boldsymbol{g}$	The homogeneous representation of $SE(3)$, $\boldsymbol{g} \in \mathbb{R}^{4\times4}$
ψ_i	The twist from the backbone bishop frame to the material frame
β_i	Arc length s where tube i is held
α_i	Absolute rotational actuation of tube i at β_i: $\psi_i(\beta_i) = \alpha_i$
ℓ_i	Total length of tube i
$\tilde{\ell}$	Arc length distance with both tubes present/precurved
k_{ib}	Bending stiffness of tube i
k_{it}	Torsional stiffness of tube i
$\mathbf{K}_i$	Stiffness map of tube i: $\mathbf{K}_i = \text{diag}(\begin{bmatrix} k_{ib} & k_{ib} & k_{it} \end{bmatrix})$
$\mathbf{K}$	Sum of the tube stiffness maps: $\mathbf{K} = \sum \mathbf{K}_i$
κ_i	Constant precurvature magnitude of tube i
$\boldsymbol{u}_i$	Curvature of tube i in material-attached frame
$\boldsymbol{u}_i^*$	Precurvature of tube i in material-attached frame
$\boldsymbol{e}_i$	ith standard basis vector
θ	Relative twist angle: $\theta = \psi_2 - \psi_1$
θ_{tip}	Relative twist angle at $s = L^\dagger$: $\theta_{tip} = \theta(L^\dagger)$
θ_β	Relative twist angle at actuators: $\theta_\beta = \psi_2(\beta_2) - \psi_1(\beta_1)$
h	Allowable variation function
$\mathbb{S}$	Stability metric: $\mathbb{S} > 0 \implies$ stable

the material-attached frames rotate with the torsion in each component tube, while the backbone Bishop frame does not rotate about its z-axis, by definition. A schematic of the frame assignments and kinematic symbols are shown in Fig. 1, and the variables required for the remainder of this section are given in Table I.

B. Strain Energy Computation

The strain energy stored in a component tube E_i is related to the square of its change in curvature $\Delta\boldsymbol{u}_i$ and is given by

$$E_i = \int_{\beta_i}^{\beta_i+\ell_i} \Delta\boldsymbol{u}_i^T \mathbf{K}_i \Delta\boldsymbol{u}_i \, ds \, , \tag{1}$$

where the change in curvature $\Delta\boldsymbol{u}_i(s)$ is defined as the difference between the tube's deformed curvature vector $\boldsymbol{u}_i(s)$ and the tube's undeformed precurvature vector $\boldsymbol{u}_i^*(s)$. The total strain energy stored in a configuration is the sum of the energy stored in each tube, and the matrix $\mathbf{K}_i$ is a diagonal matrix of tube stiffnesses, as given in Table I.

To compute the change in curvature of each tube $\Delta\boldsymbol{u}_i(s)$, we must know how the tubes are twisted, i.e., the functions $\psi_1(s)$ and $\psi_2(s)$ (see Fig. 1). It is convenient to look at this twisting as the difference between the twists of the individual tubes, so let us define the variable $\theta(s) = \psi_2(s) - \psi_1(s)$. The relative twisting $\theta(s)$ is governed by the following second order initial value problem.

$$\theta'' = c\sin(\theta), \;\; \theta(\tilde{\ell}) = \theta_{tip}, \;\; \theta'(\tilde{\ell}) = 0 \, , \tag{2}$$

where c is a constant given by

$$c = \kappa_1\kappa_2 \frac{k_{1b}k_{2b}(k_{1t}+k_{2t})}{k_{1t}k_{2t}(k_{1b}+k_{2b})} \, . \tag{3}$$

By numerically integrating (2) backwards in arc length from $s = \tilde{\ell}$ (where the initial conditions are known) to $s = 0$, $\theta(s)$ can be found. The curvature vectors of each tube $\boldsymbol{u}_1(s)$ and $\boldsymbol{u}_2(s)$ are algebraically related to $\theta(s)$ as

$$\begin{aligned} \boldsymbol{u}_1 &= \mathbf{K}^{-1}\Big(\mathbf{K}_1\boldsymbol{u}_1^* + \mathbf{K}_2(\mathbf{R}_\theta\boldsymbol{u}_2^* - \theta'\boldsymbol{e}_3)\Big) \quad && s \in [0,\tilde{\ell}] \\ \boldsymbol{u}_2 &= \mathbf{R}_\theta^T\boldsymbol{u}_1 + \theta'\boldsymbol{e}_3 && s \in [0,\tilde{\ell}] \end{aligned} \tag{4}$$

Behind the front plate, the tubes are straight and twist at a constant rate in arc length, so that the curvature vectors in this section are given by

$$\begin{aligned} \boldsymbol{u}_1 &= -\theta'(0)\mathbf{K}^{-1}\mathbf{K}_2\boldsymbol{e}_3 \quad && s \in [\beta_1, 0) \\ \boldsymbol{u}_2 &= \theta'(0)\mathbf{K}^{-1}\mathbf{K}_1\boldsymbol{e}_3 && s \in [\beta_2, 0) \end{aligned} \tag{5}$$

For completeness, we also know that when the inner tube is exposed, its curvature is equivalent to its precurvature, or

$$\boldsymbol{u}_1 = \boldsymbol{u}_1^* \quad s \in (\tilde{\ell}, \beta_1 + \ell_1] \tag{6}$$

For the problem we are considering, both tubes have a constant precurvature beginning at $s = 0$, so their precurvature functions are given as

$$\begin{aligned} \boldsymbol{u}_1^*(s) &= \begin{cases} \mathbf{0} & s \in [\beta_1, 0) \\ \kappa_1\boldsymbol{e}_1 & s \in [0, \beta_1 + \ell_1] \end{cases} \\ \boldsymbol{u}_2^*(s) &= \begin{cases} \mathbf{0} & s \in [\beta_2, 0) \\ \kappa_2\boldsymbol{e}_1 & s \in [0, \beta_2 + \ell_2] \end{cases} \end{aligned} \tag{7}$$

Since the local curvature of each tube $\boldsymbol{u}_i$ and its precurvature $\boldsymbol{u}_i^*$ are known at every arc length, the change in local curvature $\Delta\boldsymbol{u}_i$ can be found for each tube, and the strain energy can be computed from (1).

C. Stability

Until recently, it was unclear how the mechanics-based model of concentric tubes could be used to predict elastic instability. The gap in this understanding has been filled by [12], [13] which go through this issue in detail. In [12], stability is examined from a variational perspective, and a stability metric $\mathbb{S}$ is proposed. This stability metric is a scalar that is positive when a given concentric tube manipulator configuration is stable, negative when the configuration is unstable (and, therefore, not physically realizable), and zero when a snap occurs. The stability metric can be found by integrating an initial value problem, where the state variable is an allowable variation function $h(s)$, over the arc length interval $s \in [0, \tilde{\ell}]$.

$$h'' = c\cos(\theta)h, \;\; h(\tilde{\ell}) = 1, h'(\tilde{\ell}) = 0 \, . \tag{8}$$

$h(s)$ and $\theta(s)$ from equation (2) can be found simultaneously by combining (2) and (8) into an initial value problem and numerically integrating. The result of this integration can be used to compute the stability metric $\mathbb{S}$ as

$$\mathbb{S} = h(0) + \beta_{eq}h'(0) \, , \tag{9}$$

where

$$\beta_{eq} = \frac{\beta_1 k_{2t} + \beta_2 k_{1t}}{k_{1t} + k_{2t}} \, . \tag{10}$$

D. What Happens During Instability?

Perhaps the simplest way to understand what happens during instability is by examining an S-curve, which was first proposed as a stability analysis tool in [11], as shown in Fig. 2 (Left). The S-curve demonstrates how the relative torsional angle at the tip of the manipulator θ_{tip} maps to the relative torsional angle at the actuators θ_β. To generate the S-curve,

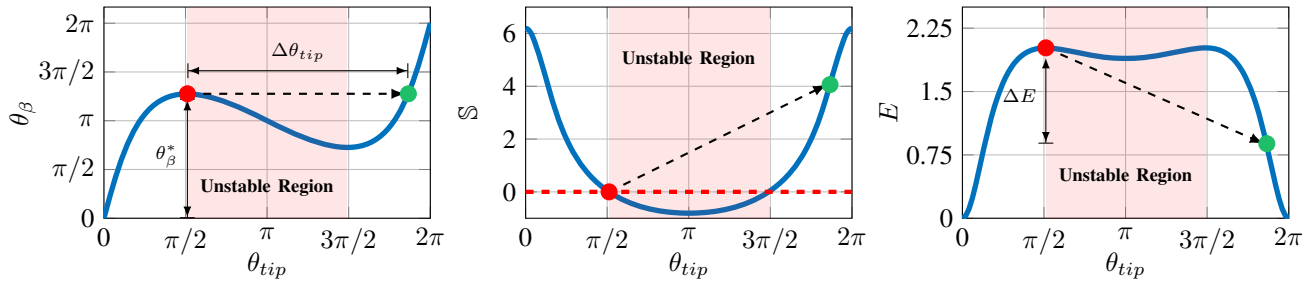

Fig. 2: In each of the plots, the unstable configurations are indicated by ▭, and the configuration that the manipulator snaps from and to are indicated by ● and ●, respectively. The dashed arrow - - ► indicates the sudden snap from the critically stable configuration to the new, stable configuration. (Left) The S-Curve shows the mapping from tip relative angle θ_{tip} to actuator relative angle θ_β. $\Delta\theta_{tip}$ gives the change in relative tip angle that occurs during instability, while θ^*_β indicates the actuator relative angle when the snap occurs. (Center) The stability metric $\mathbb{S}$ is shown for each configuration. The red dashed line - - - indicates the critical stability threshold, and all configurations below this line are unstable. (Right) The strain energy stored in the manipulator is shown for each configuration. The energy released during the snap is denoted with ΔE.

θ_{tip} is discretized from $[0, 2\pi]$, and equation (2) is integrated for each value, generating a new θ_β each time. If the tubes experience no torsional moments, the S-curve would simply be a line $\theta_\beta = \theta_{tip}$. The morphing of this line into the S-curve is dictated by the torsional energy storage in the tubes.

Each value of θ_{tip} uniquely defines a configuration of the concentric tube manipulator (though some of those configurations are unstable). The same cannot be said for the relative actuation angle θ_β, as shown in Fig. 2 (Left), some values of θ_β map to multiple values of θ_{tip}. During a 360° rotation of the tubes with respect to each another, the actuators force θ_β to move from 0° to 360°. As the robot moves, θ_β begins by moving stably from 0° until it approaches θ^*_β. The moment the actuators command θ^*_β, stability $\mathbb{S}$ goes to zero as shown in Fig. 2 (Center), and an elastic instability occurs. Without changing θ_β, the system snaps to a new θ_{tip} value. The system does this because there is a direction it can move (i.e. an allowable variation) to reduce stored energy by ΔE, as it snaps from its critically stable configuration to a lower energy, stable configuration, as shown in Fig. 2 (Right). Our goal is to convert this energy into the work required for driving a suture.

III. Experiments

This section begins by exploring the design space for a two-tube manipulator that is capable of driving a suturing needle. From this analysis, we then select three example designs, which deliver a range of powers during an elastic instability. These designs are subsequently evaluated in parallel throughout the remainder of the experiments.

A. Design Space Evaluation and Tube Selection

Since suturing needles have a constant curvature arc shape, a pure rotation at the tip of a concentric tube robot can be used to drive the needle through tissue. As a motivating example, consider surgery in the throat where a rigid endoscope is introduced through the mouth. The goal would be to create a rotational motion to drive the arced suture needle through tissue. To accomplish this, we choose a concentric tube robot design that minimizes Cartesian motion during an elastic instability. One design that does this, which we use in the experiments that follow, is a manipulator with an outer tube that is stiffer and lower in curvature than the inner tube. We note that these choices are somewhat arbitrary, since there are likely a variety of other designs which could exhibit useful needle driving behavior. The tube parameters we selected are shown in Table II. Note that the inner tube is actually (without loss of generality) a nitinol wire which facilitates attaching the needle. We attached the needle by gluing it into a small hole drilled through the wire perpendicular to the wire axis (see Fig. 7). While this attachment method was useful for the proof-of-concept experiments herein, we note that a gripper that can both grab and release and re-grab the needle will be needed in practice for suturing. Creating such a gripper is left to future work. For ease of data analysis, we use a constant $\tilde{\ell} = 20.7\,\text{mm}$.

After these design choices had been made, two more choices remained to fully define the design: the precurvature of the inner nitinol tube and the total length of the inner nitinol tube. To inform these two design decisions, we parameterized the design space with these two variables and looked at three instability metrics: the energy released for that design ΔE, the angle that the tip of the manipulator sweeps during the snap $\Delta\theta_{tip}$, and the base angle (i.e. the motor commanded angle) when the manipulator snaps θ^*_β. Refer to Fig. 2 for the definition of the each of these variables. The resulting design spaces are shown in Fig. 3. A tip deflection limit of 0.3 mm was chosen somewhat arbitrarily as a good threshold for defining minimal tip motion during snapping. The mechanics-based model was then used to check candidate designs against this threshold, and maximum strain was also evaluated to ensure that this value remains below the plastic deformation limit at all times (see Table III).

As shown in Fig. 3 (Left) the energy released varies between viable designs from 0 to over 150 mJ. The angle that the tip sweeps ranges from 0° to over 260°. We prefer that our chosen design sweep through at least 180° in order to drive the needle through the tissue plane. The tube angle the motors must command before instability occurs ranges from 180° to over 360° for our chosen design space. This variable can be thought of as "loading" the energy into the manipulator, which will subsequently be suddenly unloaded during the instability. It is interesting to note that there are designs (not shown here) where the tubes can be wound up well over 360°, and even multiple full revolutions. Since the energy released and snap angle combination needed to adequately drive the suture were not well-known a priori, we chose three designs – each with

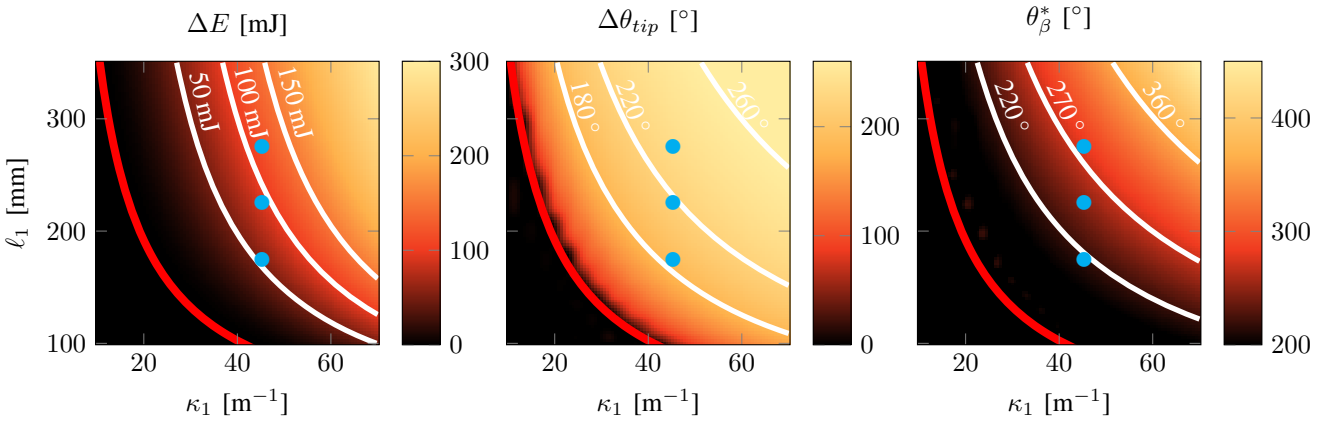

Fig. 3: The curvature of the inner tube κ_1 and the length of inner tube ℓ_1 were discretized with $\kappa_1 \in [10, 70]$ m^{-1} and $\ell_1 \in [100, 350]$ mm, each with 20 equally spaced increments. The energy released during the snap (Left), the relative angle the tip of the inner tube sweeps through (Center), and the relative angle at the base of the manipulator when the snap occurs (Right) are shown for this design space. The red line is the model predicted snapping boundary (i.e. designs left of this line are stable). The three designs evaluated experimentally are defined in Tables II and III and indicated above by ●.

TABLE II: The chosen design specifications of the tubes. The outer tube was made from SS304 while the inner tube was made from NiTi. The curved overlapping section $\tilde{\ell}$ was constrained to be 20.7 mm.

	ID	OD	κ_i	β_i
Inner Tube	0.00 mm	1.016 mm	45.3 m^{-1}	$\tilde{\ell} - \ell_1$
Outer Tube	1.24 mm	2.11 mm	9.81 m^{-1}	-24.7 mm

TABLE III: The three designs tested in the set of experiments. Other tube parameters are shown in Table II. The model-predicted deflection of the tip during the snap is indicated by δ^*_{tip}. The maximum bending strain for each design was less than 6% and the maximum torsional strain was less than 1%.

	ℓ_1	ΔE	$\Delta\theta_{tip}$	θ^*_β	δ^*_{tip}
Design 1	174.2 mm	55.1 mJ	188.7 °	216.2 °	0.29 mm
Design 2	224.2 mm	90.0 mJ	217.0 °	247.0 °	0.28 mm
Design 3	274.2 mm	117.0 mJ	234.7 °	279.2 °	0.26 mm

the same inner tube precurvature but varying total lengths – that spanned a large energy release range and evaluated each of them in parallel in subsequent experiments. The chosen designs are indicated in Fig. 3 and enumerated in Table III.

B. Power Release During Instability

The challenge, from a modeling perspective, of understanding the power released during an elastic instability is that the mechanics-based model for concentric tube robots is quasi-static. In other words, the model predicts the system configuration/energy storage before the snap, and immediately following the snap, but does not predict anything about what happens *during* the snap. A dynamic model is needed to predict the behavior of the robot during the snap, but such a model has yet to be formulated for concentric tube robots.

However, as a first step towards understanding the power available, we can combine the quasistatic model-predicted energy release and measure the time of the snap, to estimate the average power released during a snap. To measure this, we use a high speed camera (Phantom v310, Vision Research USA) to determine the duration of the elastic instabilities for each of the three chosen designs. The experimental setup is as shown in Fig. 5, but the synthetic skin was not present for this experiment. Fig. 4 shows a frame recorded from just before and just after the snap. The different designs were implemented simply by changing the location at which the inner tube was grasped, which is equivalent to changing the variable ℓ_1. The inner tube was held in a rotational stage by a collet and could be rotated precisely via a manual knob.

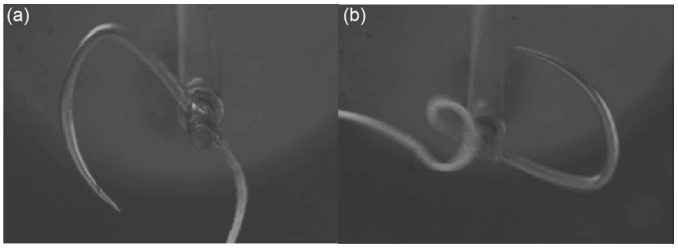

Fig. 4: (a) The moment just before the elastic instability. (b) The moment after the instability for Design 2.

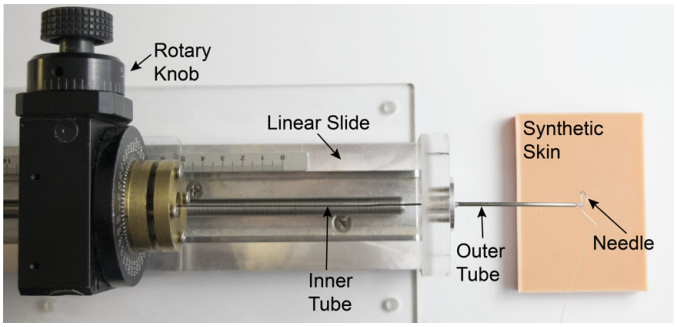

Fig. 5: The top view of the experimental setup.

Images were taken at 40,000 frames per second, and the angle of the needle was measured frame-by-frame as the snap occurred. The angular velocity of the needle was computed from these measurements, and is shown for the three designs in Fig. 8. Here, we define the start of a snap as the time when the needle's velocity reaches 20% of its maximum value. We chose this threshold because the start of a snap was challenging to identify visually and depends on a variety of factors such as friction and the speed with which the input dial was rotated by hand. We similarly defined the end of the snap as the time when the needle reaches its maximum angular velocity. Each design exhibited maximum angular velocities over 4,000 rad/s, with the needle reaching over 8,000 rad/s in the design with the highest predicted energy release. The model-predicted energy release (ΔE) was divided by the snap time to calculate an average power prediction for each experiment, as shown in Table IV. This power prediction is intended to give an ap-

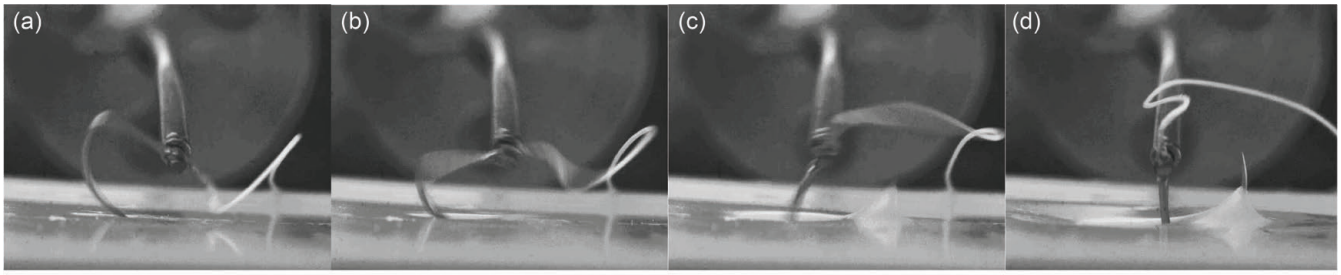

Fig. 6: A series of frames taken with the high-speed camera as the concentric tube manipulator moves through an elastic instability. These are images from the elastic instability of the configuration with the highest predicted energy release.

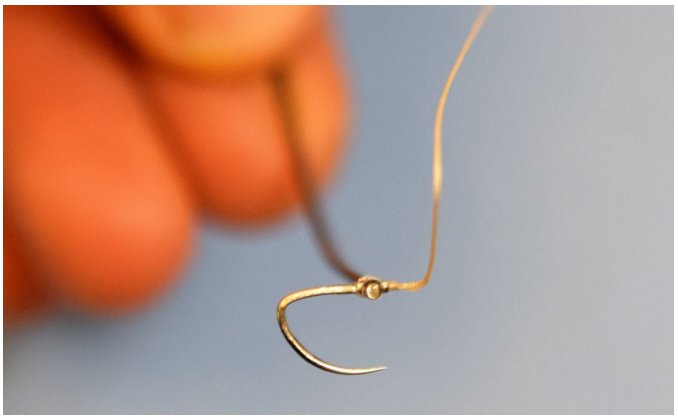

Fig. 7: Modified Suture Needle (Ethicon USA): The radial distance provided by the small bent portion gives the needle the ability to follow its tip as the inner tube of the concentric tube manipulator rotates.

proximate measure of the power delivered during a snap. This estimation yields a general idea of the power available during elastic instability, which has not previously been measured and may be useful to designers as a starting point for optimizing snaps for a specific application. These measurements may also be useful towards an experimental validation of a dynamic model for concentric tube robots.

Although the energy released during each of the instabilities is only a fraction of a Joule, because it takes place over such a short period of time, we estimate the average power available to be between 73-213 W. It is important to note that the power available at the needle tip to perform work will be somewhat less than this value because some energy will be dissipated via vibration and friction. In subsequent sections, however, we will experimentally test whether there is sufficient power to drive a curved needle through simulated tissue for each of the three designs. First, however, we evaluate whether we can produce this power at a repeatable input angle.

TABLE IV: The model predicted energy release ΔE, the observed snap time, and the resulting average power for each of the three designs. The observed snap time is defined here as the time between when the needle reaches 20% of its maximum velocity to when it reaches its maximum velocity.

	ΔE	Snap Time	Avg. Power
Design 1	55.1 mJ	0.750 ms	73.5 W
Design 2	90.0 mJ	0.575 ms	156.5 W
Design 3	117.0 mJ	0.550 ms	212.7 W

C. Repeatability of Snap Angle

The goal of this experiment was to determine whether or not the snap angle was repeatable. Model validation of the absolute snap angle has previously been assessed in [12] (see Fig. 8 of that paper). Despite this validation, the repeatability of the snap angle has yet to be fully investigated. Repeatability of the snap angle is critical if elastic instability is to be used for a surgical application. Using the same setup as used in the power experiments (see Fig. 5), we performed ten snaps for each of the three designs. To induce elastic instability, the outer and inner tube were first aligned, and then the inner tube was rotated until instability occurred. The average, maximum, and minimum actuator angle at which the snap occurred were recorded for each design. The maximum angular difference between snap angles of all of the repeatability experiments in this section was 1.2°, and the maximum standard deviation was 0.4°. The angles of snaps were consistent, and both the largest difference and largest standard deviation were associated with the configuration that had the highest predicted energy release.

D. Driving the Suture Needle Through Tissue

As mentioned in Section III-A, we designed the concentric tubes so the inner tube will achieve a nearly pure rotation. To use this rotation to drive a needle, we attached the needle to the tip of the concentric tube manipulator. We did this by drilling a 0.6 mm diameter hole in the tip of the inner tube. We then bent a small portion of a 180° suture needle (Ethicon, USA) to provide an offset that could be inserted into this hole and glued in place. The offset is approximately normal to the arc of the remainder of the needle, as shown in Fig. 7. The intent of this offset was to enable the needle path to follow its own circular arc through tissue as it is actuated by the rotation of the tip of the concentric tube manipulator. The synthetic skin to be sutured (Your Design Medical USA) was held in place and the needle was driven via elastic instability for each of the three designs. We note that in an eventual clinical embodiment, the offset would be replaced by a gripper that could grasp and release the needle in this orientation with respect to the needle tip, but we leave the design of such a gripper to future work.

For all three configurations, the needle was able to slice through the skin (see supplementary video attachment). The configuration with the lowest energy release barely delivered the needle fully through the tissue, with the tip of the needle just protruding through the skin's surface. The configuration with the highest energy release traveled through the skin rapidly and ended with a large length of needle protruding from the tissue (see Fig. 6 for a series of photos from this motion). It should be noted that these experiments consider only the first step of suturing; complete suturing will require future development of a gripper that can grasp, hold, and

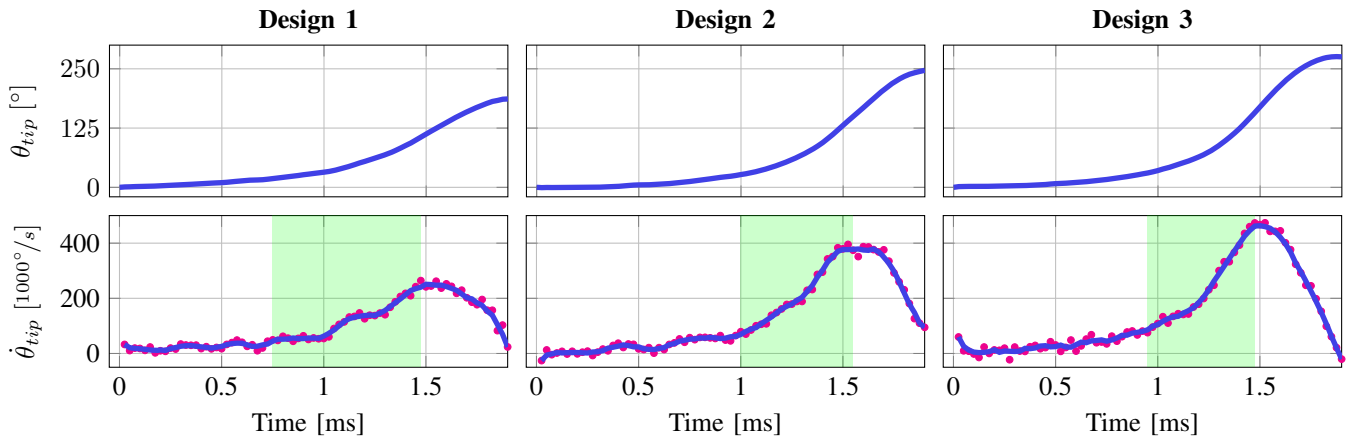

Fig. 8: The angular position and velocity of the tip of the manipulator. A moving average of the angular position is plotted and the raw angular velocity data is overlaid with a moving average. The shaded region ▭ indicates the duration of snap, with limits defined by the time when the needle has reached 20% of its maximum velocity and when the needle has reached its maximum velocity.

release the needle, as well as tie a knot when needed. The bent needle fixed to the tip of the concentric tube manipulator was used for ease of manufacturing so that the authors could focus on the feasibility studies presented in this paper, but in an actual application, a standard clinical suturing needle would be used. We envision the concentric tube manipulator equipped with a short straight rod that extends laterally from its tip and terminates in a grasper that can grasp and release the suturing needle after each suture is thrown.

IV. Discussion & Conclusion

Using elastic instabilities to perform a task may seem counterintuitive, since normally these movements are to be avoided at all costs. However, there may be instances when elastic instability could be beneficially harnessed. Perhaps one needs to cut tissue in a constrained space, and a snap could deliver the power necessary to do so. Another example would be in throwing a suture, as studied in this paper. An example of where that might be done in a manner very much like the prototype used in this paper is throwing a suture from the tip of a rigid endoscope in a deep anatomical cavity, as is the case when doing surgery in the human throat using a rigid endoscope. Here, a concentric tube robot much like the ones we used experimentally in this paper could be deployed through the endoscope's working port. Future work is needed to understand how the energy delivered to the needle will interact dynamically with tissues of various properties. Modeling this needle-tissue interaction is beyond the scope of the current paper, but is a fascinating modeling and design challenge.

These proof-of-concept experiments demonstrate the potential of using concentric tube elastic instabilities, previously viewed as undesirable events, to drive a suturing needle. This is one example of how elastic instabilities might be harnessed beneficially. We suspect that there may be other applications in minimally invasive surgery requiring high power delivery from small-diameter instruments (e.g. applying clips, staples, driving needles). The suturing concept used for proof-of-concept in this paper also still clearly requires additional advancements before it can be practically applied in surgery. Most importantly, a gripper must be developed that can grasp and release the needle, and the suture must be tied at the end, potentially using the same or a similar grasper. Still, the results in this paper show for the first time how the energy generated in an elastic instability can be harnessed beneficially, and may inspire future use of elastic instability to perform other beneficial minimally invasive surgical tasks.

References

[1] H. Azimian, P. Francis, T. Looi, and J. Drake, "Structurally-redesigned concentric-tube manipulators with improved stability," *IEEE/RSJ Int. Conf. Intelligent Robots and Systems*, pp. 2030–2035, 2014.

[2] J. Kim, D. Lee, K. Kim, S. Kang, and K. Cho, "Toward a solution to the snapping problem in a concentric-tube continuum robot: Grooved tubes with anisotropy," *IEEE Int. Conf. Robot. Autom.*, pp. 5871–5876, 2014.

[3] J. Ha, F. Park, and P. Dupont, "Achieving elastic stability of concentric tube robots through optimization of tube precurvature," *IEEE/RSJ Int. Conf. Intelligent Robots and Systems*, pp. 864–870, 2014.

[4] P. J. Swaney, H. B. Gilbert, R. J. Hendrick, O. Commichau, R. Alterovitz *et al.*, "Transoral steerable needles in the lung: How non-annular concentric tube robots can improve targeting," in *Hamlyn Symp. Medical Robotics*, 2015.

[5] J. Ha and P. E. Dupont, "Designing stable concentric tube robots using piecewise straight tubes," *IEEE Robotics and Automation Letters*, vol. 2, no. 1, pp. 298–304, 2017.

[6] C. Bergeles, A. H. Gosline, N. V. Vasilyev, P. J. Codd, P. J. del Nido *et al.*, "Concentric tube robot design and optimization based on task and anatomical constraints," *IEEE Trans. Robot.*, vol. Electronic Pre-Print, pp. 1–18, 2015.

[7] K. Leibrandt, C. Bergeles, and G. Z. Yang, "Implicit active constraints for safe and effective guidance of unstable concentric tube robots," in *Intelligent Robots and Systems (IROS), 2016 IEEE/RSJ International Conference on*. IEEE, 2016, pp. 1157–1163.

[8] K. Leibrandt, C. Bergeles, and G. Z. Yang, "Concentric tube robots," *IEEE Robotics & Automation Magazine*, vol. 1070, no. 9932/17, 2017.

[9] K. Leibrandt, C. Bergeles, and G. Z. Yang, "On-line collision-free inverse kinematics with frictional active constraints for effective control of unstable concentric tube robots," in *Intelligent Robots and Systems (IROS), 2015 IEEE/RSJ International Conference on*. IEEE, 2015, pp. 3797–3804.

[10] D. C. Rucker, B. A. Jones, and R. J. Webster, III, "A geometrically exact model for externally loaded concentric tube continuum robots," *IEEE Trans. on Robot.*, vol. 26, pp. 769–780, 2010.

[11] P. E. Dupont, J. Lock, B. Itkowitz, and E. Butler, "Design and control of concentric-tube robots," *IEEE Trans. Robot.*, vol. 26, no. 2, pp. 209–225, 2010.

[12] H. B. Gilbert, R. J. Hendrick, and R. J. Webster III, "Elastic stability of concentric tube robots: A stability measure and design test," *IEEE Transactions on Robotics*, vol. 32, no. 1, pp. 20–35, 2016.

[13] J. Ha, F. C. Park, and P. E. Dupont, "Elastic stability of concentric tube robots subject to external loads," *IEEE Transactions on Biomedical Engineering*, vol. 63, no. 6, pp. 1116–1128, 2016.